AMERICAN
METEOROLOGICAL
SOCIETY

Bulletin of the American Meteorological Society

The DOI for this manuscript is doi: 10.1175/BAMS-D-13-00084.1

The CHUVA Project – how does convection vary across Brazil?

Luiz A. T. Machado[1], Maria A. F. Silva Dias[2], Carlos Morales[2], Gilberto Fisch[3], Daniel Vila[1], Rachel Albrecht[1], Steven J. Goodman[4], Alan Calheiros[1], Thiago Biscaro[1], Christian Kummerow[5], Julia Cohen[6], David Fitzjarrald[7], Ernani Nascimento[8], Meiry Sakamoto[9], Christopher Cunningham[1], Jean-Pierre Chaboureau[10], Walter A. Petersen[11], David Adams[12], Luca Baldini[13], Carlos F. Angelis[1], Luiz F. Sapucci[1], Paola Salio[14], Henrique M. J. Barbosa[15], Eduardo Landulfo[16], Rodrigo F. Souza[17], Richard J. Blakeslee[18], Jeffrey Bailey[19] , Saulo Freitas[1], Wagner. F. A. Lima[1] and Ali Tokay[20]

1. Instituto Nacional de Pesquisas Espaciais (INPE). Centro de Previsão de Tempo e Estudos Climáticos (CPTEC), Brazil.
2. Universidade de São Paulo. Instituto de Astronomia, Geofísica e Ciências Atmosféricas, Brazil.
3. Departamento de Ciências e Tecnologia Espacial. Instituto de Aeronáutica e Espaço, Brazil
4. National Oceanic and Atmospheric Administration (NOAA/NESDIS/GSFC), USA
5. Colorado State University, Cooperative Institute for Research in the Atmosphere, USA
6. Universidade Federal do Pará. Instituto de Geociências, Brazil.
7. University at Albany, SUNY, Atmospheric Sciences Research Center, USA
8. Universidade Federal de Santa Maria, Departamento de Física, Brazil
9. Fundação Cearense de Meteorologia, Brazil
10. Laboratoired'Aérologie, University of Toulouse, France
11. NASA Wallops Flight Facility, USA
12. Universidad Nacional Autónoma de México, Centro de Ciencias de la Atmósfera, Mexico
13. CNR Istituto di Scienze dell'Atmosfera e del Clima, Italy
14. Universidade e Buenos Aires, Argentina
15. Universidade de São Paulo. Instituto de Física, Brazil
16. Instituto de Pesquisas Energéticas e Nucleares, Brazil.
17. Universidade do Estado do Amazonas, Brazil.
18. NASA Marshall Space Flight Center, Huntsville, Alabama USA
19. University of Alabama in Huntsville, Huntsville, Alabama USA
20. University of Maryland Baltimore County Baltimore, Maryland, USA

BAMS-D-13-00084

Submitted to Bulletin of the American Meteorological Society

September, 2013.

ABSTRACT

CHUVA, meaning “rain” in Portuguese, is the acronym for the C*loud processes of tHe main precipitation systems in Brazil: A contribUtion to cloud resolVing modeling and to the GPM (GlobAl Precipitation Measurement)*. The CHUVA project has conducted five field campaigns; the sixth and last campaign will be held in Manaus in 2014. CHUVA's main scientific motivation is to contribute to the understanding of cloud processes, which represent one of the least understood components of the weather and climate system. The five CHUVA campaigns were designed to investigate specific tropical weather regimes. The first two experiments, namely, Alcantara and Fortaleza in northeast Brazil, focused on warm clouds. The third campaign, which was conducted in Belem, was dedicated to tropical squall lines that often form along the sea-breeze front. The fourth campaign was in the Vale do Paraiba of southeastern Brazil, which is a region with intense lightning activity. In addition to contributing to the understanding of cloud process evolution from storms to thunderstorms, this fourth campaign also provided a high fidelity total lightning proxy dataset for the NOAA GOES-R program. The fifth campaign was carried out in Santa Maria, southern Brazil, a region of intense hailstorms associated with frequent mesoscale convective complexes. This campaign employed a multi-model high resolution ensemble experiment. The data collected from contrasting precipitation regimes in tropical continental regions allow the various cloud processes in diverse environments to be compared. Some examples of these previous experiments are presented to illustrate the variability of convection across the tropics.

Capsule

CHUVA reveals very diverse cloud processes in tropical continental regions and contributes to improving satellite precipitation estimation, nowcasting, cloud resolving models and the understanding of cloud electrification.

1. Introduction

The CHUVA project began in 2010 and has conducted five field campaigns; the last experiment will be held in Manaus as part of *GoAmazon (Green Ocean Amazon),* in 2014 (see http://campaign.arm.gov/goamazon2014/ for a detailed description). CHUVA's main scientific motivation is to contribute to the understanding of cloud processes, which represent one of the least understood components of the climate system.

Brazil has an area of 8.5 million km^2 and lies primarily south of the Equator and within the tropics. Therefore, Brazil is ideally situated for studying tropical continental convection over a broad range of precipitation regimes within a single country. In the Northeast Brazil, a semi-arid region, the CHUVA project was designed to characterize warm clouds (Costa et al., 2000) and the organized convection influenced by the inter-tropical convergence zone and easterly waves (Kouadio al., 2012). Cotton (1982) defines warm clouds as clouds in which the ice phase does not play a substantial role in the precipitation process. In the Amazon, specifically in the Belem and Manaus regions, the main targeted precipitation regimes were tropical squall lines (Cohen et al., 1995); local convection, which is strongly forced by the diurnal cycle (Machado et al. 2002); and mesoscale convective systems (Rickenbach, 2004). In southern Brazil, at the boundary of the tropical and subtropical regions, CHUVA measured the convection associated with cold fronts (Garreaud, 2000), mesoscale convective complexes (Salio et al., 2007) and strongly electrified convection (Cecil and Blankenship, 2012). The field campaigns in each of these regions collected detailed observations of various

rainfall regimes over a tropical continental region to improve our understanding of cloud processes. The campaigns focused on the following applications: satellite precipitation estimation, cloud resolving models, nowcasting and cloud electrification. CHUVA is contributing to the National Aeronautics and Space Administration (NASA) - Japan Aerospace Exploration Agency (JAXA) Global Precipitation Measurement (GPM), National Oceanic and Atmospheric Administration (NOAA) Geostationary Operational Environmental Satellite R-series (GOES-R) and GoAmazon Programs.

Schumacher and Houze (2003) demonstrated large seasonal and regional variability in the stratiform rain fraction (the contribution of stratiform precipitation to the total precipitation) over Brazil using the TRMM precipitation radar. Precipitation estimation has been noticeably improved by the Tropical Rainfall Measuring Mission (TRMM) and the development of new algorithms (Tapiador et al., 2012). However, precipitation estimation over land using passive radiometers still has several deficiencies. Specifically, precipitation is indirectly estimated (Berg et al., 2006). Moreover, precipitation from warm clouds is largely underestimated, especially when using microwave radiometers, and contributes (7.5% on average) to the total rainfall in tropical coastal regions (Liu and Zipser, 2009). Over land, microwave satellite precipitation estimates exploit the relationship between ice aloft and rainfall at the surface. Because these clouds have no ice, the precipitation estimates for warm cloud rainfall are inaccurate. For example, during November 2008, 283 mm of rainfall, mostly from orographic warm clouds, was measured by rain gauge over twenty-four hours in southeastern Brazil. However, only very light precipitation amounts (approximately 30 mm) were estimated using satellite data

(Silva Dias, 2009). Williams and Stanfill (2002) discuss the formation of warm cloud rainfall in the context of cloud condensation nuclei and updrafts and contrast the marine and continental environments.

The passive microwave rainfall sensors used by the GPM constellation to achieve three-hour rainfall estimates have largely relied on ice scattering signals to convert brightness temperature depressions into rainfall rates over continental regions. The CHUVA field campaigns, in addition to their focus on the microphysical properties of tropical clouds, have an important role in improving existing algorithms for precipitation retrieval for the Global Precipitation Measurement mission. Therefore, an important component of CHUVA was to provide a homogeneous dataset to the community that supports GPM algorithm development in both warm and cold phase clouds. As mentioned, warm rain clouds are particularly challenging for the passive microwave remote sensing of precipitation. CHUVA data will help address this issue.

The dataset collected in this project, combined with cloud modeling, is expected to create a solid basis for the development of improved database on cloud process over the continental tropics. This dataset contains hydrometeor classifications, thermodynamics profiles, rainfall drop size distributions and several remote sensing (both active and passive) cloud property measurements. Realistic parameterizations of cloud processes are a prerequisite for reliable current and future climate simulations. Meteorological models, at very high resolution, explicitly describe cloud processes to a large degree; however, the cloud microphysics and turbulent processes require parameterization. Morrison et al. (2007) demonstrate the large sensitivity of high–resolution simulations to the

microphysical parameterizations. The CHUVA dataset, combining model, satellite, radar, radiometer and other in-situ data, will provide an opportunity to validate and improve cloud resolving models over various tropical continental regions.

GOES-R, the next generation of NOAA geostationary satellites, includes a new capability for total lightning detection from the Geostationary Lightning Mapper (GLM). The GLM will aid in forecasting severe storms, tornadic activity and will address convective weather impacts on aviation safety and efficiency (Goodman et al., 2013). The CHUVA measurements provide a high fidelity dataset for GLM application development in continental tropical regions.

This study outlines the motivation for developing the CHUVA project and general information on the measurement strategy and how to access the database and the project webpage. Additionally, this study presents a specific description of each field experiment, a discussion of the preparation for the final campaign, and a summary of the main results and activities for project outreach.

2. Motivation

CHUVA's principal motivation is the description and understanding of the cloud processes of the various precipitation regimes of Brazil. The expected results include improved satellite precipitation estimates, especially from warm clouds; cloud resolving model evaluation; development of nowcasting techniques for intense thunderstorms; and an improved understanding of the cloud electrification processes in the tropics/sub-tropics. The CHUVA project addresses the following questions:

- *How can satellite estimates of warm cloud precipitation be improved?*
- *How can GPM satellite-based retrievals of rainfall over the continent be improved?*
- *What are the typical cloud processes that occur in the main precipitation regimes of Brazil?*
- *What are the major surface and boundary layer processes relevant to the formation and maintenance of clouds?*
- *What are the primary processes in the evolution from shallow to deep convection and how do cloud microphysical and electrification processes evolve during this transition and cloud life cycle?*
- *How can the representation of clouds and accuracy be improved in cloud resolving models, especially for* intense thunderstorms*?*
- *How can all of the acquired knowledge be utilized to improve nowcasting and forecasting in tropical regions?*

To answer these questions, the CHUVA Project focused on collecting data that describes the multi-dimensional structure of clouds in different precipitation regimes. These data include: a) The selected cloud properties from XPOL and MRR data; b) satellite and radar precipitation fields, cloud type classification and cloud and rain cell life cycles; c) the electric fields and lightning associated with clouds from the lightning network and field mills (an electro-mechanical device which measures the strength of the electrostatic field at the surface), which are essential for describing thunderstorm electrification processes; and d) mesoscale atmospheric conditions and surface fluxes from rawinsondes and from towers to

assess the atmospheric dynamical and thermodynamic properties. These data are combined with a cloud resolving model (the Brazilian version of the Regional Atmospheric Modeling System - BRAMS) to describe the typical cloud processes of the various precipitation regimes. As proposed by Negri et al. (2013), comparing satellite and/or radar measurements with virtual images simulated by radiative transfer and cloud resolving model outputs can validate the model and create a microphysical database.

These datasets are specifically used to (1) test different methodologies for estimating warm cloud precipitation, (2) evaluate the possible relationships between integrated ice content, electrification and precipitation as functions of the cloud life stage, (3) employ different satellite rainfall algorithms and assess the associated regional errors, (4) describe the temporal evolution of the electrical field during thunderstorm development in conjunction with the radar polarimetric variables, (5) investigate the column-integrated atmospheric water vapor during periods preceding intense thunderstorms and (6) analyze the capability of cloud resolving models to describe the microphysical properties and the effect of the turbulence parameterization on cloud organization.

3. Experimental Design

a) Sites and Measurement Strategies

CHUVA consists of six field campaigns, five of which have already taken place. The sixth will be carried out in 2014 in Manaus as part of the GoAmazon initiative

154 (http://campaign.arm.gov/goamazon2014/). Figure 1 (left panel) shows the
155 experimental sites of the CHUVA projects and illustrates the main precipitation
156 regime expected in each region. Figure 1 (right panel) shows a schematic
157 representation of the measurement strategy employed in the CHUVA campaigns. A
158 primary instrument used for CHUVA is a mobile X-band dual polarization radar (X-
159 Pol). Schneebeli et al. (2012a and 2012b) give a detailed description of the radar,
160 operation and data processing. The radar scan strategy consists of a volume scan
161 with 10 to 14 elevations (depending on the main type of clouds targeted) and at
162 least one Range-Height Indicator (RHI) scan along the direction of the main
163 instrumentation site. The RHI is performed with an antenna rotation rate of nine
164 degrees per second, a high angular resolution (every 0.50°) and a high sampling
165 frequency (obtained using 150 samples per ray) to ensure a high vertical resolution
166 and data accuracy. The entire procedure (strategy) also includes a differential
167 reflectivity (Zdr) offset check using a vertical measurement along the column above
168 the radar. Figure 1 presents a typical description of the measurement strategy. The
169 distance between the radar site and the main site is approximately 20 km; the
170 main site is equipped with the following basic instruments (see Table I for a
171 detailed description): impact (Joss-Valdwogel) and laser (OTT Parsivel and Thies)
172 disdrometers; rain gauges (tipping bucket employed in a dual gauge configuration
173 at the main site); a microwave radiometer (MP3000A with 35 channels) ranging
174 from 22.00 to 30.00 GHz (21 channels), range associated with water vapor
175 emissions, and from 51.00 to 59.00 GHz (14 channels), range associated with
176 molecular oxygen emissions (Ware et al., 2003). Additionally, the main site
177 instrumentation includes one vertically pointing K-Band (24.1 GHz) micro rain radar

178 (MRR) (see Peter et al. (2005) for a detailed description), a Raman lidar at 532/604
179 nm, a GPS dual-frequency receiver to retrieve the column-integrated atmospheric
180 water (Sapucci et al., 2007), a field mill and a surface weather station to measure
181 surface latent and sensible heat fluxes, soil moisture and temperature. In addition
182 to the main site, two to four other sites instrumented with disdrometers, rain
183 gauges, a GPS receiver and field mills (variable number) were installed at various
184 distances from the radar. Rawinsondes were routinely released (at least twice a
185 day). During specific intensive observation periods (IOPs), a triangle of rawinsondes
186 in a nearly equilateral arrangement was launched 4 times a day (00:00, 06:00,
187 12:00 and 18:00 UTC).
188
189 **b) Data Access and the CHUVA Web Page**
190
191 The CHUVA website – http://chuvaproject.cptec.inpe.br – is the primary access to
192 the CHUVA information and data. For each campaign, a specific webpage was
193 developed (Figure 2). These web pages contain a wide variety of information
194 including the daily weather report, instrument strategy, instrument locations, quick
195 looks of the main events, data reports, cloud pictures and the SOS-CHUVA (Severe
196 storm Observation System), a geographical information system that utilizes data
197 from the CHUVA project and allows retrospective access to the radar, satellite and
198 model images, when available. The use of SOS-CHUVA for nowcasting will be
199 discussed in more detail in section 5. The CHUVA dataset has been pre-processed
200 and is available through the CHUVA website. Data can be accessed at different
201 levels. For example, level 0 data from the X-band radar are raw data in ASCII and

202 universal format (UF), level 1 data consist of the attenuation-corrected (Zh and Zdr)
203 data in ASCII and UF (see Testud et al., 2000, for a detailed description of the
204 attenuation correction), and level 2 data consist of the corrected reflectivity
205 constant altitude plan position indicators (CAPPIs) at various altitude levels.
206 Additional corrections, such as the correction for bias due to a wet radome and the
207 ZDR offset adjustment, are not applied in this dataset. However, instructions and
208 tables are accessible to the users for their own applications. Data for each
209 instrument comes with a "readme" file with information about the data and how
210 to manipulate the files. All raw data and several processed data (level 2) are
211 publicly available through the CHUVA website.
212 In addition, the CHUVA datasets for each campaign include the available
213 operational S-band radar data covering the field campaign region (see Table I for a
214 description of additional instrumentation), the GOES and Meteosat geostationary
215 satellite images (infrared channels) and all overpasses of the operational
216 environmental low-orbiting satellites carrying passive microwave sensors (channels
217 similar to TRMM-TMI).
218
219 **4. Field Campaigns**
220
221 **a) Alcantara**
222
223 Alcantara was the first CHUVA campaign from March 1-25, 2010. In addition to the
224 array of CHUVA instruments, the Alcantara experiment employed the Advanced
225 Microwave Radiometer for Rain Identification (ADMIRARI) (see Battaglia et al.

226 (2011) for a detailed description). The ADMIRARI measurements consist of passive
227 radiances collected at vertical and horizontal polarization at frequencies of 10.7,
228 21.0 and 36.5 GHz, and one co-staring active radar (MRR). The ADMIRARI were
229 pointed at a fixed 30° elevation angle oriented along a radial directed toward the X-
230 Pol radar located at a range of 7.65 km. Along the line between the X-Pol radar and
231 the ADMIRARI, two additional sites measured rainfall and drop size distributions.
232 Three distinct weather conditions were observed during the campaign. During the
233 first period (1 to 9 March) the convection was suppressed with only scattered
234 clouds and sparse rainfall. The second period (10 to 16 March) was characterized
235 by the beginning of the wet season with isolated local convection and dominant
236 warm cloud processes. The last period (16 to 25 March) experienced intense
237 convection with warm and deep (cold cloud/ice phase) convection, with
238 precipitation rates as high as 150 mm h^{-1}, the 99^{th} percentile corresponds to 137
239 mm h^{-1} (the rain rate information described in this study was computed using rain
240 gauge tipping buckets integrated over one-minute intervals). The warm rainfall
241 events in Alcantara were associated with the highest concentration of large drops
242 (larger than 4 mm). Battaglia et al. (2011) describes two precipitation events during
243 the campaign in which the 21.0 and 36.5 GHz channels and the MRR were
244 repeatedly saturated with heavy rain. In one event, the 10 GHz signal was
245 saturated, which was the first time the ADMIRARI operation ever observed
246 saturation on this channel (this was the third ADMIRARI campaign). TRMM co-
247 located 2A25 version-7 near-surface precipitation radar was compared against the
248 precipitation measured during the CHUVA campaign by rain gauge. Alcantara
249 precipitation estimation from TRMM is underestimated by more than 50%. Of all

250 the campaigns to date, Alcantara has the highest average rainfall rate from warm
251 clouds (7.2 mm h^{-1}), one of the largest vertically integrated water vapor values and
252 high cloud water contents for non-precipitating clouds (0.34 mm), only slightly
253 smaller than observed in Belem. Alcantara also has the highest CAPE; the 99^{th}
254 percentile corresponds to 1950 J Kg^{-1}.
255
256 **b) Fortaleza**
257
258 The data collection period spanned April 3-28, 2011, during the rainy season. The
259 main site was installed in the yard of the Civil Defense Organization (the
260 organization responsible for responding to natural disasters) in Fortaleza. A
261 partnership with Fundação Cearense de Meteorologia e Recursos Hídricos
262 (FUNCEME) was established for monitoring intense thunderstorms. The X-Pol radar
263 was installed in the city of Osorio, 20.5 km from the main CHUVA site. Additionally,
264 three more sites with disdrometers, rain gauges and GPS receivers were installed
265 around Fortaleza, and the most distant was 32.6 km from the radar. Given that the
266 focus of this campaign was warm cloud processes and deep convection associated
267 with the inter-tropical convergence zone (ITCZ), a volume scan strategy was
268 implemented with thirteen elevations focusing on both the lower and upper
269 troposphere (i.e., warm and deep cloud types). As already mentioned, the strategy
270 for all campaigns included a Zdr offset check and RHIs scans. For Fortaleza, two
271 RHIs scans were performed: one over the main site and another at 180 degrees,
272 perpendicular to the coast, where most systems propagate into the continent.
273 Three complete scans (volume scan, RHIs and vertically pointing) were run in 20-

minute cycles and a zero check (background noise estimation) was performed once per hour.

Rawinsondes were launched in Fortaleza every six hours. However, in the time interval of April 8-17, two additional sites located 135 km away in the cities of Quixeramobim and Mossoró were added, and these began to launch rawinsondes concurrently. This nearly equilateral triangular sounding array was designed to cover mesoscale systems penetrating the continent. During this period, multiple organized convective systems crossed the array in succession.

The maximum rainfall intensity recorded during the campaign was 152 mm h^{-1}, with the drop size distributions (DSDs) revealing a large population of large (> 4 mm) raindrops. Fortaleza had the largest average vertically integrated water vapor (56.1 mm) and the highest melting level (4.7 km). These characteristics suggest that the rainfall events in Fortaleza appear to have a very important warm process when producing rain drops. Additionally, the stratiform rainfall in Fortaleza exhibited the highest and least prominent bright-band (BB) peak intensity (Calheiros and Machado, 2013). Fortaleza had the second highest CAPE; the 99th percentile corresponds to 1840 J Kg^{-1}.

c) Belem

The Belem campaigns was performed during the period June 1-30, 2011, toward the end of the wet season and during the period of maximum squall line frequency (see Garstang et al. (1994) and Cohen et al. (1996) for a detailed description on Amazonian squall lines). Negri et al. (2000) used a satellite-derived gauge-adjusted

precipitation climatology from microwave measurements, i.e., the Goddard Profiling algorithm. They found a persistent local rainfall maximum at 1800 LST, which moved inland at 21:00 LST, due to interactions between sea-breeze and squall line formation and propagation into the Amazon along the northern coast of Brazil.

The X-Pol radar was installed on the roof of the Meteorology Department of the Federal University of Pará along the Guama River, a tributary of the Amazonas River. Two main sites were set up, one in Outeiro and another in Benevides, 23.0 and 27.7 km from the radar, respectively. In general, rawinsondes were launched twice daily in Belem, with the exception of an intensive observation period from June 18-26, during which four rawinsondes were launched daily in the cities of Tomé Açu and São Miguel, approximately 120 km apart. The radar volume scan strategy was similar to that used in the previous experiments. Additionally, within the ten-minute scan period strategy, ten more RHIs were performed (separated by 1.5 degrees) perpendicular to the Amazonas River covering the rawinsondes triangle network. In addition to the typical CHUVA instrumentation, a mesoscale GPS meteorological network was established (Adams et al. 2011) with fifteen stations in close proximity (a 5 km to 10 km separation distance within Belem and a 40 km distance outside of Belem). This GPS network provided very high spatial and temporal resolution for the column-integrated atmospheric water vapor and its variability. Additionally, three field mill sensors were installed at Belem and the main sites. Finally, controlled meteorological (CMET) balloons (Voss et al. 2005) were launched from Tomé-Açu, Pará. These balloons are altitude controlled via satellite, and the winds were determined using GPS tracking and a package carrying

temperature and moisture sensors. Two CMETs were launched twelve hours apart. The CMET measurements, i.e., temperature and relative humidity, show the same boundary layer structure as the Tomé-Açu rawinsondes. Each CMET was recovered. The CMETs landed in the Tocantins River after six hours of flight. During the flights, a mesoscale convective system to the south led to a strong directional wind shear in the lower layers. Preliminary numerical studies using the BRAMS model employing back trajectory are consistent with a southerly flow in response to a depression associated with the interaction of a mesoscale convective system and a developing sea breeze, which also promoted a southerly flow.

Several squall lines formed along the coast and sea breeze front, propagating inland over the Amazonian rainforest, as described earlier by Cohen et al. (1995). However, several of the observed squall lines were not initiated along the coast but along the boundary of the rain forest and the semi-arid region to the east of Belem. These squall lines propagated almost parallel to the coast. Another interesting feature was the multi-scale nature of these large squall lines. Embedded in the large cloud deck, successively smaller scale propagating rainfall cell lines were detected by the radar. Figure 3 displays one example of the consecutive RHI scans through the squall line on June 7, 2011. A typical vertical cross-section of the evolving squall line is apparent; initially shallow warm clouds develop, followed by rapidly deepening clouds up to 14 km. Following the convective region, the stratiform sector evolved with a clear bright-band and a cloud top approximately 13 km at 22:00 UTC. During the dissipation phase (cloud collapse), the cloud top height decreases and the bright-band region intensifies. The bright-band signature is the result of complex microphysical processes that occur when snowflakes melt

346 in stratiform precipitation (Fabry and Zawadsky, 1995). More than twenty rain
347 events crossed the experimental region; the rain rate at the 99th percentile was
348 122 mm h^{-1}. The CAPE was also very high. However, the CAPE was less than at
349 Alcantara and Fortaleza; the 99th percentile corresponds to 1380 J Kg^{-1}.
350
351 **d) Vale do Paraíba**
352
353 The Vale do Paraíba campaign had the longest duration, with an IOP from
354 November 1 to December 22, 2011, followed by a second period with less intensive
355 measurements continuing through March 31, 2012. The instrumentation was
356 installed along a line perpendicular to the coast. The radar was 90 km inland from
357 the ocean at an elevation of 650 m. The main site was installed 11 km from the X-
358 Pol radar, and a succession of sites (spaced by approximately 20 km) was installed
359 along a line perpendicular to the ocean. These sites had at least one GPS IPW
360 (Integrated Precipitable Water) station, one disdrometer and multiple rain gauges.
361 Additionally, five field mills, spaced 1 km apart, formed a very high spatial
362 resolution array close to the radar. The radar strategy was designed to run for six
363 minutes.
364 During November and the first week of December, the region had an anomalous
365 southeasterly flow, decreasing the air temperature and increasing convective
366 inhibition. From the second week of December to March, several intense
367 thunderstorms and some severe weather events were reported in the region.
368 The primary objective of this campaign was to study storm electrification. As such,
369 comprehensive ground-based measurements of total lightning activity were

collected to improve our understanding and knowledge of thunderstorm initiation and behavior and also develop more advanced nowcasting tools that combine radar, lightning, satellite and numerical weather prediction (Goodman et al., 2012). The second objective was to conduct cross-network inter-comparisons and capability assessments of operational and research ground-based regional 2-D and 3-D total lightning mapping networks that might be useful for merging with or validating the space-based lightning measurements becoming available late this decade. This specific component of the field experiment included a very successful collaboration among Brazilian, US, and European organizations (from universities and industry). The participating lightning location systems (LLSs) were STARNET (Sferics Timing And Ranging NETwork), RINDAT (Rede Integrada Nacional de Detecção de Descargas Atmosféricas), WWLLN (World Wide Lightning Location Network), ATDnet (Arrival Time Difference network), Vaisala GLD360 (Global Lightning Dataset) and TLS200 (Total Lightning Sensor), BrasilDAT (Sistema Brasileiro de Detecção de Descargas Atmosféricas), LINET (Lightning Network), and LMA (Lightning Mapping Array). The last four networks were deployed along a short baseline for total (intracloud and cloud-to-ground) lightning detection in support of the development of proxy datasets and validation protocols in preparation for the next generation of operational weather satellites (Goodman et al., 2013) and the Meteosat Third Generation Lightning Imager in 2018 (Holler et al., 2013). The lightning measurements provided by these LLSs were made concurrently with overpasses of the TRMM Lightning Imaging Sensor (LIS) and the SEVIRI (Spinning Enhanced Visible and Infrared Imager) on the Meteosat Second Generation satellite. A 10-station Lightning Mapping Array network, expanded to

394 twelve stations in early December and then providing near-real time data, was
395 deployed over the eastern region of the Vale do Paraiba in the vicinity of São Paulo
396 to be one of the references for total lightning measurements. The distance
397 between the LMA stations was 15-30 km, and the network "diameter" was
398 approximately 60 km. Bailey et al., (2011) discuss a similar LMA configuration that
399 provides accurate 3-D lightning mapping and good detection efficiency as far as
400 150 km from the network center. This specific network installed in CHUVA has no
401 information about the specific efficiency detection; this information will be
402 available only after the cross-network inter-comparisons.
403 The combined lightning, satellite and radar data provide the most comprehensive
404 dataset to date. The dataset prepares users for the next generation of
405 geostationary satellite imagery and lightning mappers using SEVERI and LIS
406 measurements. Figure 4 presents an example of the characteristic lightning data
407 collected during one overpass of the TRMM satellite. The LMA, as well as the LIS,
408 were able to detect and locate lightning from various sub-components of individual
409 flashes.
410 Additionally, nowcasting applications were tested based on detailed information of
411 intense thunderstorms that produced hail, damaging winds and flooding over the
412 metropolitan area of São Paulo and Vale do Paraiba. Figure 5 provides an example
413 of a severe weather event that produced very large hail (up to 20 mm) and flooding
414 in the region. A rapid increase in lightning source numbers, known as the
415 "lightning-jump", firstly discussed by William et al., (1999), is associated with
416 severe weather, occurred in advance of the hail event. Figure 5A shows the 15-
417 minute accumulated LMA source density (number of sources in a 1x1 km^2 grid

418 during a 15-minute period) plotted in latitude-longitude, latitude-height and
419 longitude-height projections and the observed signature of the lightning-jump. This
420 cell was initiated southwest of Sao Paulo and traveled through Sao Paulo and
421 Guarulhos cities with reflectivities greater than 40 dBZ from 1700 to 1830 UTC,
422 reaching values greater than 65 dBZ at 1745 UTC when hail was reported in
423 downtown Sao Paulo. Moreover, 15 minutes later, hail and flooding were reported
424 in Guarulhos, which corresponds with the maximum observed LMA sources (Figure
425 5B). The electrical structure of this cell exhibited two well-developed charge
426 centers with maximum activity near 1800UTC. This lighting source maximum
427 (lightning-jump) and has been associated with severe weather, including tornados
428 (Schultz et al., 2009). The lightning activity had two major source regions at
429 approximately 7 km and 10 km. These thunderstorms extended to a height of 18
430 km. Cloud electrification is tightly controlled by updrafts and precipitation
431 formation. Therefore, monitoring lightning activity inside a cloud can lead to severe
432 weather warnings detected by a lightning-jump signature.
433 The LMA mapped the convective cells in near real-time. The most recent 10
434 minutes of the LMA lightning data were uploaded to the CHUVA nowcasting
435 website (SOS) every 5 minutes. This site provides civil defense, management
436 organizations, electrical power companies and the public with information on real-
437 time convection and lightning threat.
438 During the Vale do Paraiba campaign, several intense thunderstorms and some
439 severe weather events were recorded, including a downburst, causing destruction
440 of many trees, and many cases of hailstorms. The rain rate at the 99^{th} percentile at
441 the main site was 137 mm h^{-1}. Warm clouds during the Vale do Paraiba campaign

had a lower frequency and average rain rate than the others CHUVA tropical sites. Moreover, non-precipitating clouds exhibited a small average measured value (0.13 mm) and the largest difference with the adiabatic calculation. One possible reason for this finding is the dry entrainment effect that reduces the liquid water content below the estimated adiabatic value. The CAPE value at vale do Paraiba was nearly identical to the observations in Belem; the 99th percentile corresponds to 1260 J Kg^{-1}. The Vale do Paraiba and Santa Maria locations had a very small average integrated water vapor amount (27 and 29 mm, respectively) compared with the sites located closer to the equator.

e) Santa Maria

The Santa Maria campaign, named CHUVA SUL, took place from November 5 to December 12, 2012. Zipser et al. (2006) report that very intense thunderstorms are observed in this region and mesoscale convective systems organized by the penetration of cold fronts are common. Liu et al. (2010) used a 10-year satellite database from TRMM to show that most precipitation in this region (more than 2000 mm/year) comes from thunderstorms. During the campaign, the rain rate at the 99th percentile was 106 mm h^{-1}. Six mesoscale convective systems crossed the region during the campaign, with intense activity confined primarily to Argentina and Uruguay. On 1 December, a convective event brought down trees near the main site and was considered the most intense storm crossing the sites. Unfortunately, the X-band radar suffered a voltaic arc and could not be repaired in time for the campaign. However, two S-band radars operated by the Brazilian Air

466 Force, one in Santiago and another in Cambuçu, 100 km and 180 km from the main
467 site, respectively, made measurements during this event. These radars ran a
468 volume scan strategy, employing 15 elevations every ten minutes. All of the CHUVA
469 instruments were installed similar to the other campaigns using rainfall
470 measurement sites, a GPS mesoscale network and a field mill network. Additional
471 instrumentation included surface weather stations in a mesoscale network
472 composed of six stations spaced 20 km apart. The rawinsondes were launched
473 twice a day. During the occurrence of organized systems, soundings were also
474 launched every six hours in Santiago and Cruz Alta, approximately 120 km apart.
475 The Santa Maria campaign showed the lowest value for CAPE; the 99^{th} percentile
476 corresponds to only 400 J Kg^{-1}, larger values were only observed closed to the six
477 main events. A unique activity in CHUVA SUL was the use of the High Resolution
478 Limited Area Model Ensemble (HRLAMENS). The HRLAMENS effort was developed
479 under mutual collaboration between CHUVA and the LPB-RDP (La Plata Basin -
480 Research and Development Project, which focuses on high impact weather), which
481 aimed to furnish additional information on the total amounts and locations of
482 precipitation and their uncertainties. The HRLAMENS was composed of five models
483 (two versions of the BRAMS model and three versions of the Weather Research
484 and Forecasting (WRF) model), which were integrated using the Centro de Previsão
485 de Tempo e Estudos Climáticos (CPTEC) supercomputing facilities. Moreover, four
486 others model configurations were ran in others Institutions in Brazil and Argentina.
487 This core set of models was designed to be driven by selected global ensemble
488 prediction system members from CPTEC and the National Centers for
489 Environmental Prediction. The simulations were homogeneous in domain size and

horizontal and vertical resolution (2 km grid spacing and 41 levels). Partner institutions in the project assisted with the multi-model composition in their respective model (WRF running in University of Buenos Aires, WRF running at University of Santa Maria and MESO-NH from the Laboratoire d'Aerologie (France)). The results are still being evaluated. Nevertheless, preliminary conclusions indicate, as expected, sensitivity to the lateral boundary conditions and model characteristics. The ultimate objective is to find an optimal balance among ensemble members that would improve the current state of rainfall predictions for the region.

f) GoAmazon - Manaus.

The GoAmazon experiment seeks to understand the interaction of aerosol and cloud life cycles. The GoAmazon experiment will be performed in Manaus, a megacity of almost 1.8 million people in the central Amazon. Two intensive operating periods (IOP) are being prepared for 2014, one in February-March, during the wet season, and another in September-October, at the end of the dry season. The GoAmazon experiment consists of several combined efforts, including the deployment of the ARM mobile facility (Cadeddu et al., 2013), the Grumman Gulfstream 159 (G-1) aircraft (from the Pacific Northwest National Laboratory) to collect chemistry and microphysical properties, ACRIDICON (Aerosol, Cloud, Precipitation, and Radiation Interactions and Dynamics of Convective Cloud Systems) with the High Altitude and Long Range Research Aircraft (HALO), which is the new research aircraft of the German Science Community (Gulfstream G-550)

514 and the CHUVA project. The CHUVA campaign will employ an X-Pol measurement
515 strategy, which provides volume scans and several RHIs over the sites in
516 coordination with the ARM cloud radar. It is important to note that the GPM core
517 observatory will be launched during the first IOP. Hence, there will be an
518 opportunity to combine data from the TRMM and GPM core satellites with those
519 collected during GoAmazon to study cloud and precipitation processes over one of
520 the rainiest continental regions of the planet.
521
522 **5. CHUVA Outreach**
523
524 **a) The CHUVA-SOS Nowcasting system**
525
526 The SOS-CHUVA is a web-based geographic information system combining
527 observations from radar, lightning networks, satellite images, numerical models
528 and nowcasting procedures. This is a useful tool to interpret, summarize and
529 integrate the environmental information and display and send warnings for
530 emergency management groups. In addition, SOS_CHUVA is an open access system
531 serving the population through real time information, thereby reducing citizen
532 vulnerability. By taking advantage of the instrumentation employed in each
533 campaign, a nowcasting pilot project is set up for each region, which addresses
534 specific vulnerabilities and needs. The SOS-CHUVA provides high resolution radar,
535 satellite and lightning data nearly in real time. It also provides the results from
536 several nowcasting applications, including the radar forecast for the next ten
537 minutes (based on Fortracc, Vila et al., 2007, and the Rainbow data processing

538 system software) and the lightning probability (Machado et al., 2009), among
539 several other functions, such as the total integrated precipitation for each
540 neighborhood. For the regions outside of the radar coverage, the system provides
541 information based on the hydroestimator and the Fortracc nowcasting cloud
542 systems for the following two hours using geostationary satellite data. The system
543 also provides forecast data from the BRAMS cloud resolving model at a resolution
544 of a few kilometers. The SOS-CHUVA in each campaign was developed in
545 partnership with the local civil defense and fire departments.
546
547 **b) Training and Education and Workshop**
548
549 Outreach activities are an important component of the CHUVA project. For
550 example, training lectures were presented to local students during each campaign
551 via a one-week course that covered themes of nowcasting, cloud resolving models,
552 polarimetric radar, satellite data usage, lidar, GPS and cloud microphysics. The
553 lectures were offered to graduate and undergraduate students in environmental
554 sciences; more than 100 students attended each campaign course. The programs
555 and details of each course are available from the specific webpage of the campaign.
556 Finally, an international workshop was organized in May 2013 in São Paulo. Access
557 to the abstracts and the presentations is available at the following URL:
558 http://chuvaproject.cptec.inpe.br/portal/workshop/index.html.
559
560 **6. Discussion.**
561

562 The use of similar instruments across campaigns in the various precipitation
563 regimes makes it possible to study the regional contrasts and correspondences.
564 Figure 6 illustrates examples of similarities and differences among the various
565 precipitation regimes. Figure 6A shows the DSD adjustment to the gamma function
566 (using the momentum method described by Tokay and Short, 1996) in the three-
567 dimensional space of the gamma parameters: the intercept (N_0) in the x axis, the
568 shape (m) in the y axis and the width (Λ) in the z axis, using the same procedure
569 employed by Cecchini et al. (2013). In this three-dimensional space (a logarithmic
570 option is applied to N_0 to adjust the data to the same range), the DSD gamma
571 parameters are represented for the Vale do Paraiba, Belem and Santa Maria
572 campaigns. Each point in this diagram corresponds to a specific DSD. We note the
573 regional differences in the frequency of occurrence over the gamma parameter´s
574 spatial domains. However, it is very interesting to see that all points, regardless of
575 the regime, are nearly over the same adjusted surface. Therefore, we can
576 parameterize the Gamma distribution using only two independent parameters. The
577 raindrop size distribution characteristics observed by surface based disdrometers
578 can distinguish different precipitation systems. Tokay et al. (2002) demonstrated
579 the presence of more large drops and small concentration in easterly regime than
580 in the westerly regime in the southwestern Amazon basin. In their study, DSD
581 differences were also observed between the monsoon and break regimes in
582 Northwest Australia. The DSD features from CHUVA will be analyzed in detail after
583 the completion of the GoAmazon project.
584 Another example of regional contrasts/similarities is presented in Figure 6B using
585 the warm cloud-ice cloud index (WII). The WII is defined as the ratio of the

586 difference between the cloud thickness of the cloud layer below and above the
587 freezing level and the total cloud thickness (see Figure 6b for a schematic view and
588 the associated equation). The WII was computed using the vertical profile of
589 reflectivity (VPR) by employing data from the X-Pol RHI scanning mode and the co-
590 located rawinsondes (+-3 hour interval) over the main site. Only continuous cloud
591 layers were considered in this analysis; multi-layer clouds were discarded. A
592 continuous layer cloud was defined as having a continuous layer with values larger
593 than 0 dBZ in the warm sector and -10 dBZ in the layer above the 0°C isotherm.
594 Different thresholds were used because ice has a smaller refractive index than
595 liquid water. All rain events (rain rate greater than 0.1 mm h^{-1}) from non-
596 multilayers clouds and when rawinsonde data were available were computed in
597 the WII analysis. The thickness of the layer under the melting layer (L1) was defined
598 as the layer between the lifting condensation level (LCL) and the melting level
599 (both obtained from rawinsondes). The LCL is used to avoid possible rain layers
600 detected by the radar below the cloud base. The parameter L2, characterizing the
601 layer above the melting layer, is defined as the thickness of the layer between the
602 melting level and the last level of the continuous layer of reflectivities larger than -
603 10 dBZ. L2 roughly represent the cloud layer above 0°C isotherm, because radar
604 does not detect the cloud boundaries. The WII ranges from 1 (a pure warm cloud)
605 to -1 (clouds associated only with ice and/or supercooled water). Figure 6b
606 presents the rainfall cumulative frequency for each WII value. The cumulative
607 rainfall is obtained from a disdrometer located at the main site along the RHI
608 azimuth direction employed to build the VPR. The population for each site (rainfall
609 cases at the main site were associated with a single layer cloud that occurred

610 within the six-hour interval centered on the rawinsonde launch time) is variable,
611 ranging from 116 in Alcantara to 1500 Vale do Paraiba, depending on the number
612 of rainy days, the frequency of multilayer clouds and the duration of the campaign.
613 The cumulative rainfall, for each site, is presented as function of the WII values in
614 Fig. 6b to give an information about the specific cloud population of WII values in
615 the total rainfall. Two different behaviors can be observed in Fig. 6b.The first
616 behavior corresponds to negative WII values, responsible for approximately 70%-
617 75% of the total precipitation amount. Vale do Paraiba and Belem exhibit deep
618 clouds with a layer L2 above the melting level that is nearly three times larger (a
619 WII value of approximately -0.5) than the warm layer L1; for Fortaleza and
620 Alcantara, this layer is only 1.5 times larger than the warm layer (a WII around -0.3).
621 The second behavior, accounting for the remaining 30%-25% of precipitation, is
622 nearly linearly distributed for the positive values of the WII, expect for Vale do
623 Paraiba. These clouds are characterized by rain processes that are primarily below
624 the melting layer. Alcantara, Belem and Fortaleza present a very similar behavior;
625 approximately 25% of the precipitation is from clouds with most of their thickness
626 below the melting layer (associated with warm processes). However, the Vale do
627 Paraiba rainfall events display a different behavior, in which a very small portion,
628 i.e., less than 5%, of the rainfall is associated with warm clouds. This clearly shows
629 a distinction between coastal and continental rainfall events; a different population
630 of rainfall events from warm clouds was observed. This difference could be reason
631 of cloud process in the clean maritime air near the coast and the more polluted air
632 inland.

633 Another regional comparison was performed to evaluate cloud organization using
634 GOES satellite images. Figure 6c shows the cumulative distribution of the
635 convective cloud fraction (defined as 10.7 μm Brightness Temperature smaller than
636 235 K) as a function of the cloud cluster effective radius (an equivalent area circle;
637 effective radius = $(\text{Area}/\pi)^{1/2}$). This convective cloud size distribution only includes
638 clouds with very high cloud tops, i.e., colder than 235 K. Therefore, no warm clouds
639 are included. The calculation was performed using the same procedure as
640 employed by Machado and Rossow (1993) over a region centered on the main site
641 with a radius of 250 km. The regional convective cloud size distributions are very
642 similar. Approximately 80% of the convective cloud fraction is explained by cloud
643 organization with radii smaller than 31 km for all regions. Only slight regional
644 differences are noted for convective cloud organization smaller than 31 km
645 effective radius. Alcantara and Belem have fewer small convective clouds than the
646 others sites. Moreover, Vale do Paraiba exhibits more moderately sized systems
647 (approximately 31 km). However, the largest difference is for convective cloud
648 organization larger than 31 km. Santa Maria has the largest cloud organization,
649 probably due to the more baroclinic instability favoring large MCCs and cold fronts.
650 The CHUVA dataset has just begun to be explored, but some clear regional
651 characteristics can already be described. The warm clouds in Alcantara feature very
652 large droplets (disdrometer measurement) and high liquid water contents
653 (microwave radiometer). Several pixels that were classified as stratiform due to the
654 presence of a bright-band exhibiting large reflectivities and rain rates values. It is
655 possible that the ice aloft, prior to the bright-band formation, is sufficiently
656 vigorous to produce larger rain rates than expected for normal stratiform cloud

conditions. The largest CAPE found in Alcantara could explain this strength in the ice production. The highest and most prominent bright-band was observed in Alcantara, which agrees with this notion. Deep convective clouds in Fortaleza display the largest amount of rain water below the melting layer. Costa et al. (2000) showed different DSDs for maritime, coastal, continental and polluted warm clouds in the Fortaleza region. They demonstrated a pronounced increase in concentration and decrease in the maximum droplet diameter as the clouds moved from the ocean to the continent into polluted regions. The high CAPE for these coastal sites helps the development of deep convection. However, these coastal tropical sites have more warm rain clouds and less deep convection than the Vale do Paraiba and Santa Maria locations. Several processes must be considered, such as the small concentration of Cloud Condensation Nuclei (CCN) at the coastal sites. Moreover, the larger trade wind inversion could contribute suppressing deep convection and increase warm cloud formation.

The deepest clouds were recorded in Santa Maria, Belem and Vale do Paraiba. These are the regions of very deep clouds, often with cloud tops above 15 km, and organized convection with a more dominant ice phase. Belem presented the most developed glaciated layer (above 7 km), whereas Vale do Paraiba displayed the most developed mixed phase layer, i.e., between the melting layer and 7 km (Calheiros and Machado, 2013).

7. Summary.

CHUVA provides a comprehensive dataset characterizing the main precipitation regimes in Brazil. The project consistently uses a core complement of instrumentation for each campaign and has recorded and made available high spatial and temporal resolution observations (ground and satellite based) of cloud and precipitation characteristics.

CHUVA field campaigns around the tropical region of Brazil provide education and training with respect to the employed instrumentation and the physical processes describing cloud and rainfall formation. CHUVA takes advantage of the instrumentation to present a nowcasting test-bed based on the SOS-CHUVA. The CHUVA data are available through the website, which includes all of the information on each campaign, daily reports, data strategy, quick looks, instrument locations and photos.

The CHUVA project contributes to the GLM effort to develop algorithms based on the planned GOES-R and METEOSAT third generation lightning sensors and the preparation of the GPM validation and algorithm development. The large number of warm rain clouds measured in various regions is an important resource for the satellite precipitation algorithms, especially for GPM, to test the ability of retrieving rainfall from non-ice scattering clouds over land.

Open access to the database will certainly contribute to improving the knowledge of clouds over tropical regions and advance the description and parameterization of cloud processes.

8. Acknowledgement

703 This work was supported by FAPESP grant No. 2009/15235-8, CHUVA Project and
704 CNPQ No. 573797/2008 (Brazilian National Institute of Science and Technology for
705 Climate Change). Special thanks to Mário Figueiredo for maintaining the CHUVA
706 database, Claudinei Camargo for assisting in figure preparation, Jorge Melo and
707 Jorge Marton for their engineering support during the field campaigns, Moacir
708 Lacerda, Evandro Anselmo and João Neves for their support during lightning
709 installation and Izabelly Carvalho for processing the disdrometer dataset. The
710 authors acknowledge the anonymous reviewers and the comments provided by
711 Earle Williams. The authors would also like to thank all of the participants in the
712 CHUVA field campaigns that contributed directly or indirectly during the years of
713 field work.

9. References

Adams,D.K.,R.Fernandes,E.R.Kursinski,J.Maia,L.Sapucci,L.Machado,I.Vitorello,K.Holub,S.Gutman,NazianoFilizola,R.Bennett,2011:A Dense GNSS Meteorological Network for Observing Deep Convection in the Amazon, Atmospheric Science Letters, DOI:10.1002/asl.312

Bailey, J. C., L. D. Carey, R. J. Blakeslee, S. J. Goodman, R. I. Albrecht, C. A. Morales, and O. Pinto, Jr., 2011: São Paulo Lightning Mapping Array (SP-LMA): Deployment and Plans. Proceedings XIV International Conf. on Atmospheric Electricity, Rio de Janeiro, Brazil.

Battaglia, A., P. Saavedra, C. A. Morales, and C. Simmer, 2011: Understanding 3D effects in polarized observations with the ground-based ADMIRARI radiometer during the CHUVA campaign. J. Geophys. Res.,116,D09204, doi:10.1029/2010JD015335.

Berg, W., T. L'Ecuyer, and C. Kummerow, 2006: Rainfall Climate Regimes: The Relationship of Regional TRMM Rainfall Biases to the Environment. J. Appl. Meteor. Climatol.,45, 434–454.

Cadeddu, M. P., J.C. Liljegren, and D. D. Turner, 2013: The Atmospheric Radiation Measurement (ARM) program network of microwave radiometers: instrumentation, data, and retrievals. Atmos. Meas. Tech. Discuss., 6, 3723-3763, doi:10.5194/amtd-6-3723-2013.

Calheiros, A.J.P. and L.A. T. Machado, 2013: The Cloud and Rain Liquid Water Characteristics of Different Precipitation Regimes in Brazil. Atmos. Res.

Cecchini, M. A., L.A.T. Machado, and P. E. A., 2013: Droplet Size Distributions as a Function of Rainy System Type and Cloud Condensation Nuclei Concentrations. Atmos. Res.

Cecil, D. J. and C. B. Blankenship, 2012: Toward a Global Climatology of Severe Hailstorms as Estimated by Satellite Passive Microwave Imagers. J. Climate, 25, 687–703.

Cohen, J. C. P., M. A. F. da Silva Dias, and C. A. Nobre, 1995: Environmental Conditions Associated with Amazonian Squall Lines: A Case Study. Mon. Wea. Rev., 123, 3163–3174.

Costa A. A., C. J. Oliveira, J. C. P. Oliveira, and A. J. C. Sampaio, 2000: Microphysical observations of warm cumulus clouds in Ceará, Brazil. Atmos. Res., 54, 2–3, 167-199.

Cotton, W.R., 1982 : Modification of precipitation from warm clouds-A review. Bull. Amer. Meteor. Soc., 63, 146-160.

Fabry, Frederic, Isztar Zawadzki, 1995: Long-Term Radar Observations of the Melting Layer of Precipitation and Their Interpretation. J. Atmos. Sci., 52, 838–851.

Garreaud, R. D., 2000: Cold air incursions over subtropical South America: Mean structure and dynamics. Mon. Wea. Rev., 128, 2544–2559.

Garstang, Michael, Harold L. Massie, Jeffrey Halverson, Steven Greco, John Scala, 1994: Amazon Coastal Squall Lines. Part I: Structure and Kinematics. Mon. Wea. Rev., 122, 608–622.

Goodman, S. J., J. Gurka, M. DeMaria, T. Schmit, A. Mostek, G. Jedlovec, C. Siewert, W. Feltz, J. Gerth, R. Brummer, S. Miller, B. Reed, and R. Reynolds, 2012: The GOES-R Proving Ground: Accelerating User Readiness for the Next Generation Geostationary Environmental Satellite System. Bull. Am. Meteor. Soc.,93, 1029-1040. DOI:10.1175/BAMS-D-11-00175.1.

Goodman, S. J., R. J. Blakeslee, W. J. Koshak, D. Mach, J. C. Bailey, L. D. Carey, D. E. Buechler, C. D. Schultz, M. Bateman, E. McCaul, and G. Stano, 2013: The GOES-R Geostationary Lightning Mapper. Atmos. Res., Volumes 125–126, 34-49.

Höller, H., H.-D. Betz, C.A. Morales, R. Blakeslee, J. C. Bailey and R. I. Albrecht, 2013: Multi-sensor field studies of lightning and implications for MTG-LI. 2013 EUMETSAT Meteorological Satellite Conference and 19th American Meteorological Society (AMS) satellite meteorology, oceanography, and climatology conference, September 16-20, Vienna, Austria.

Kouadio Y.K., J. Servain, L. A. T. Machado and C. A. D. Lentini, 2012: Heavy rainfall episodes in the eastern northeast Brazil linked to large-scale ocean-atmosphere conditions in the tropical Atlantic. Advances in Meteorology, 2012, ID 369567, doi 10.1155/2012/369567

Liu, C. and E.J. Zipser, 2009: Warm Rain in the Tropics: Seasonal and Regional Distributions Based on 9 yr of TRMM Data. J. Climate, 22, 767–779.

Liu, Chuntao, Earle R. Williams, Edward J. Zipser, Gary Burns, 2010: Diurnal Variations of Global Thunderstorms and Electrified Shower Clouds and Their Contribution to the Global Electrical Circuit. J. Atmos. Sci., 67, 309–323.

Machado, L. A. T., W. F. S. Lima, O. Pinto Jr, and C. A. Morales, 2009: Relationship between cloud-ground discharge and penetrative clouds: a multi-channel satellite application. Atmos. Res., 93, 304-309.

Machado L. A. T. and W. B. Rossow, 1993: Structural characteristics and radiative properties of tropical cloud clusters. Mon. Wea. Rev., 121, 3234–3260

Morrison, H. and W. W. Grabowski, 2007: Comparison of Bulk and Bin Warm-Rain Microphysics Models Using a Kinematic Framework. J. Atmos. Sci.,64, 2839–2861.

Morales, C.A., L. A. T. Machado, C. F. de Angelis, M. A. F. da Silva Dias, G. Fisch, D. Vila, J. Sakuragi, I. C. Carvalho, J.R. Neves, E.M. Anselmo, and T. Biscaro, 2013: Evaluation of TRMM PR Rainfall Estimates Over Brazil: A Contribution of CHUVA Project. Atmos. Res. (submitted).

Negri, R. G., L. A. T. Machado, S. English and M. Forsythe, 2013: Combining Cloud Resolving Model with Satellite for Cloud Process Model Simulation Validation. J. Appl. Meteor. Clim., in press.

Negri, Andrew J., Emmanouil N. Anagnostou, Robert F. Adler, 2000: A 10-yr Climatology of Amazonian Rainfall Derived from Passive Microwave Satellite Observations. J. Appl. Meteor., 39, 42–56.

Peters, G., B. Fischer, H. Münster, M. Clemens, and A. Wagner, 2005: Profiles of Raindrop Size Distributions as Retrieved by Micro rain Radars. J. Appl. Meteor., 44, 1930-1949.

Rickenbach T.M, 2004: Nocturnal Cloud Systems and the Diurnal Variation of Clouds and Rainfall in Southwestern Amazonia. Mon. Wea. Rev., 132, 1201-1219.

Salio, P., M. Nicolini and E. J. Zipser, 2007: Mesoscale Convective Systems over Southeastern South America and Their Relationship with the South American Low-Level Jet. Mon. Wea. Rev., 135, 1290–1309.

Sapucci, L. F., L. A. T. Machado, J. F. G. Monico, and A. Plana-Fattori, 2007: Intercomparison of Integrated Water Vapor Estimates from Multisensors in the Amazonian Region. J. Atmos. Oceanic Technol.,24, 1880–1894.

Schneebeli, M., J. Sakuragi, T, Biscaro, C. F. de Angelis, I. Carvalho da Costa, C. A. Morales, L. Baldini, and Machado, L. A. T, 2012a.: Observations of tropical rain with a polarimetric X-band radar: first results from the CHUVA campaign, Atmos. Meas. Tech. Discuss., 5, 1717-1761 (.doi:10.5194/amtd-5-1717-2012)

Schneebeli, M., J. Sakuragi, T. Biscaro, C. F. de Angelis, I. Carvalho da Costa, C. A. Morales, L. Baldini, and Machado, L. A. T, 2012b: Polarimetric X-band weather radar measurements in the tropics: radome and rain attenuation correction. Atmos. Meas. Tech.,5, 2183-2199.

Schumacher, Courtney, Robert A. Houze, 2003: Stratiform Rain in the Tropics as Seen by the TRMM Precipitation Radar. J. Climate, 16, 1739–1756.

Silva Dias MAF (Ed.) (2009) As chuvas de novembro de 2008 em Santa Catarina: um estudo de caso visando à melhoria do monitoramento e da previsão de eventos extremos. Nota técnica. São José dos Campos, INPE. 67p.

Schultz, Christopher J., Walter A. Petersen, Lawrence D. Carey, 2009: Preliminary Development and Evaluation of Lightning Jump Algorithms for the Real-Time Detection of Severe Weather. J. Appl. Meteor. Climatol., 48, 2543–2563.

Tapiador, F.J., F.J. Turk, W. Petersen, A. Y. Hou, E. G. Ortega, L. A. T. Machado, C. F. Angelis, P. Salio, C. Kidd, G. J. Huffman, and M. Castro, 2012: Global precipitation measurement: methods, datasets and applications. Atmos. Res.,104–105, 70-97.

Testud, J., E. Le Bouar, E. Obligis and M. Ali-Mehenni, 2000: The rain profiling algorithm applied to polarimetric weather radar, J. Atmos. Oceanic Technol., vol. 17, 322-356.

Tokay, A. and Short, D.A. Evidence from tropical raindrop spectra of the origin of rain from stratiform versus convective clouds. J. Appl. Meteorol., 35, 355-371, 1996

Tokay, A., A. Kruger, and W. Krajewski, A. Perreira, 2002: Measurements of drop size distribution in southwestern Amazon region, J. Geophys. Res., 107 (D20).

Vandenberghe, F., 2003: A multichannel radiometric profiler of temperature, humidity, and cloud liquid. Radio Sci., 38, 8079.

Vila, D. A., L. A. T. Machado, H. Laurent and I. Velasco, 2008: Forecast and Tracking the Evolution of Cloud Clusters (ForTraCC) Using Satellite Infrared Imagery: Methodology and Validation. Wea. Forecasting, 23, 233–245.

Voss, P.B., E.E. Riddle, and M.S. Smith, 2005: Altitude Control of Planetary Balloons. J. of Aircraft, 43, 478-482.

Ware, R., R. Carpenter, J. Güldner, J. Liljegren, T. Nehrkorn, F. Solheim, and F. Vandenberghe (2003). Radio Sci., 38(4), 8079, doi:10.1029/2002RS002856.

Williams, E. R., Stanfill, S. B., The Physical Origin of the Land-Ocean Contrast in Lightning Activity, Comptes Rendus Physique, Volume 3, Number 10, pp. 1277-1292, 2002.

Williams, E., R. Boldi, A. Matlin, M. Weber, S. Hodanish, D. Sharp, S. Goodman, R. Raghavan, and D. Buechler, The behavior of total lightning activity in severe Florida thunderstorms, Atmospheric Research, 51, 245-265, 1999.

Zipser, E. J., C. Liu, D. J. Cecil, S. W. Nesbitt, and D. P. Yorty, 2006: Where are the most intense thunderstorms on earth?.Bull. Amer. Meteor. Soc., 87, 1057–1071.

FIGURE CAPTIONS

Figure 1: A description of the CHUVA field campaigns over Brazil and an illustration of the main precipitation regimes. On the right, the diagram describes the reference measurement strategy adopted during the field campaigns, along with the radar site and main site with other ground instruments.

Figure 2: The CHUVA webpage (center) and examples of the data access panel (left) and the web page for the Vale do Paraiba campaign (right). Additionally, one example picture (bottom) showing the radar installation for the Vale do Paraiba campaign is shown.

Figure 3: The sequence of the RHI over a squall line crossing the main site. The illustration is presented for each hour from 17:00 to 24:00 UTC (June 7, 2011) for the Belem field campaign.

Figure 4: The coincident lightning observations on February 10, 2012 at 1900 UTC during a Lightning Imaging Sensor (LIS) overpass from approximately 19:01:10 to 19:03:24 UTC. The plotted ground-based lightning data are limited both temporally and spatially to the LIS overpass limits. The left panel shows the LIS pixels (grey squares) and the ground strikes detected by LMA VHF sources (the colored dots are function of the time). The projections east–west (top) and north-south (left) as functions of the altitude and the number of sources as a function of the altitude are also shown in the left panel.

Figure 5: A) Accumulated LMA lightning source density (number of sources in a 1x1 km grid box during a 15-minute period) for a hail-producing convective cell on 7 January 2012. The upper panels show a plan (latitude-longitude) view and the bottom panels show height-longitude views of the convective cell. Horizontal black lines in the bottom panels indicate the approximate heights of the -10^{o}C and -40^{o}C isotherms, where most of the electrical charge transfer occurs. B) Time evolution of the maximum reflectivity and the number of LMA lightning sources. Red lines indicate hail

occurrences in São Paulo and Guarulhos (the two cities showed in panels of A). Only data from the hail-producing convective cell are shown.

Figure 6: A) The DSD gamma parameters for Vale do Paraiba (black dots), Belem (brown dots) and Santa Maria (white dots) in the three-dimensional space composed by N_0, m and Λ. The color of the interpolated surface is associated with the Λ values. B) The cumulative rainfall as a function of the WII (warm cloud–ice cloud index) for Alcantara, Fortaleza, Belem and Vale do Paraiba. LCL stands for lifting condensation level. C) The cumulative convective cloud cover (Tir<235K) as a function of the cloud cluster effective radius for each campaign.

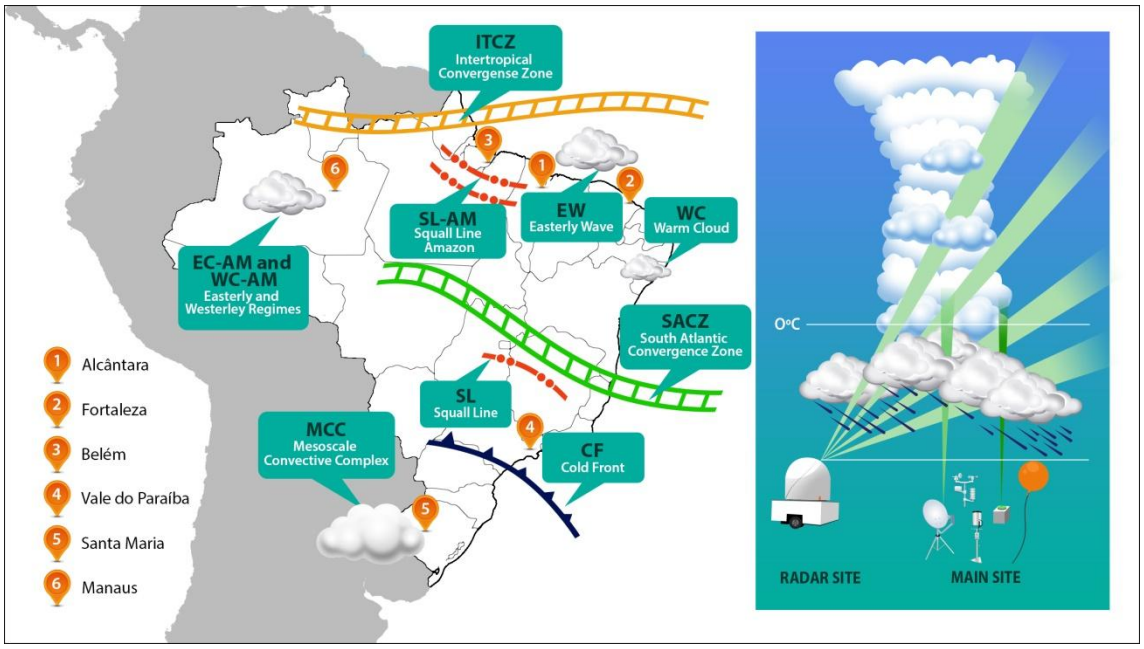

Figure 1: A description of the CHUVA field campaigns over Brazil and an illustration of the main precipitation regimes. On the right, the diagram describes the reference measurement strategy adopted during the field campaigns, along with the radar site and main site with other ground instruments.

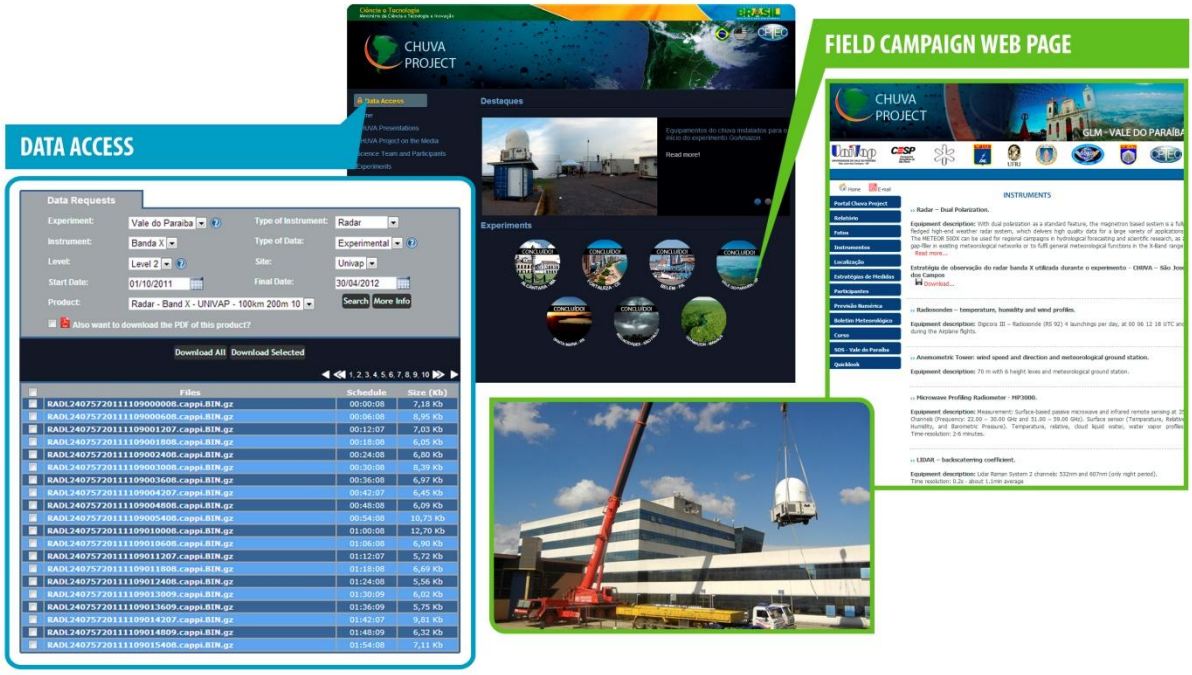

Figure 2: The CHUVA webpage (center) and examples of the data access panel (left) and the web page for the Vale do Paraiba campaign (right). Additionally, one example picture (bottom) showing the radar installation for the Vale do Paraiba campaign is shown.

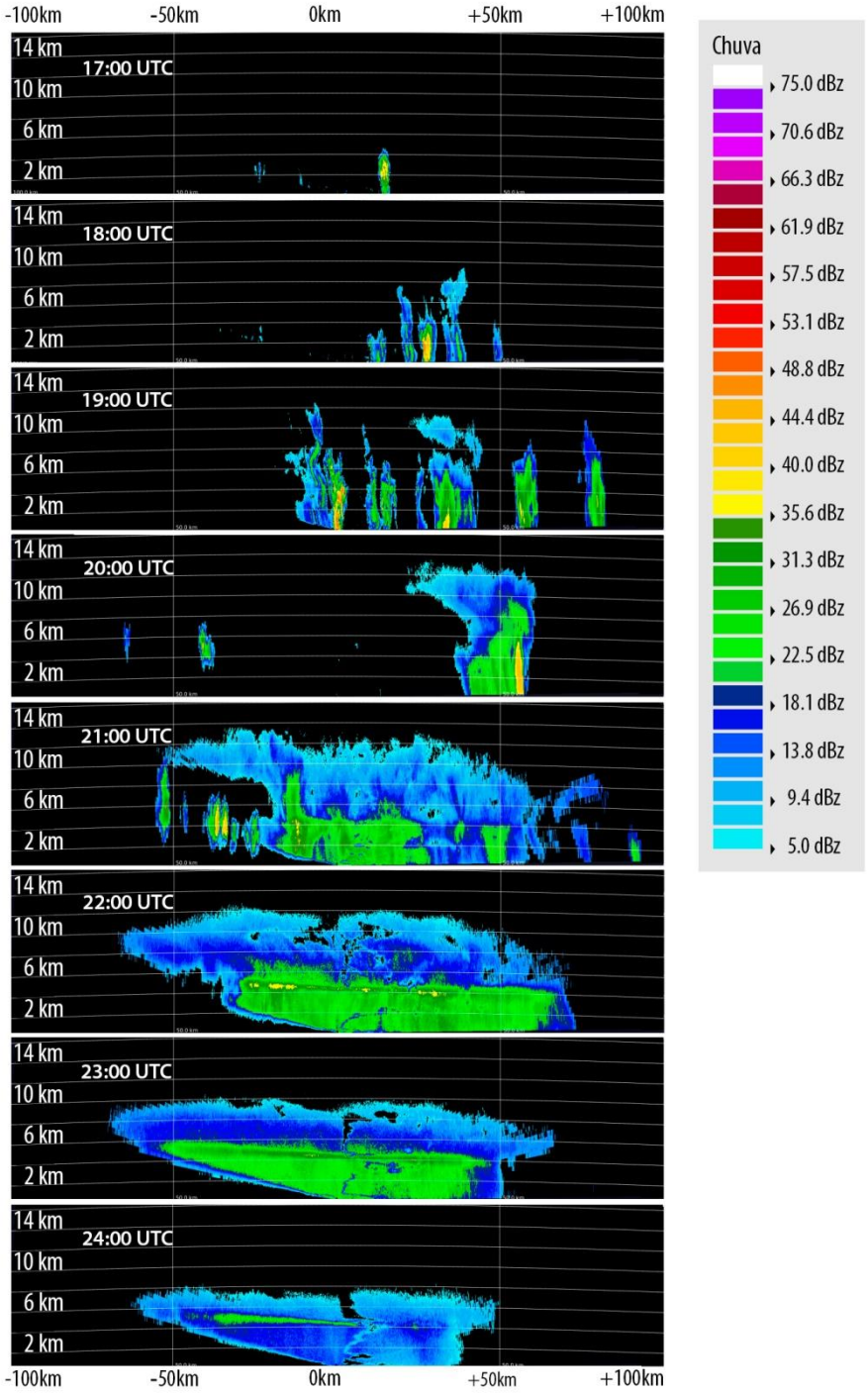

Figure 3: The sequence of the RHI over a squall line crossing the main site. The illustration is presented for each hour from 17:00 to 24:00 UTC (June 7, 2011) for the Belem field campaign.

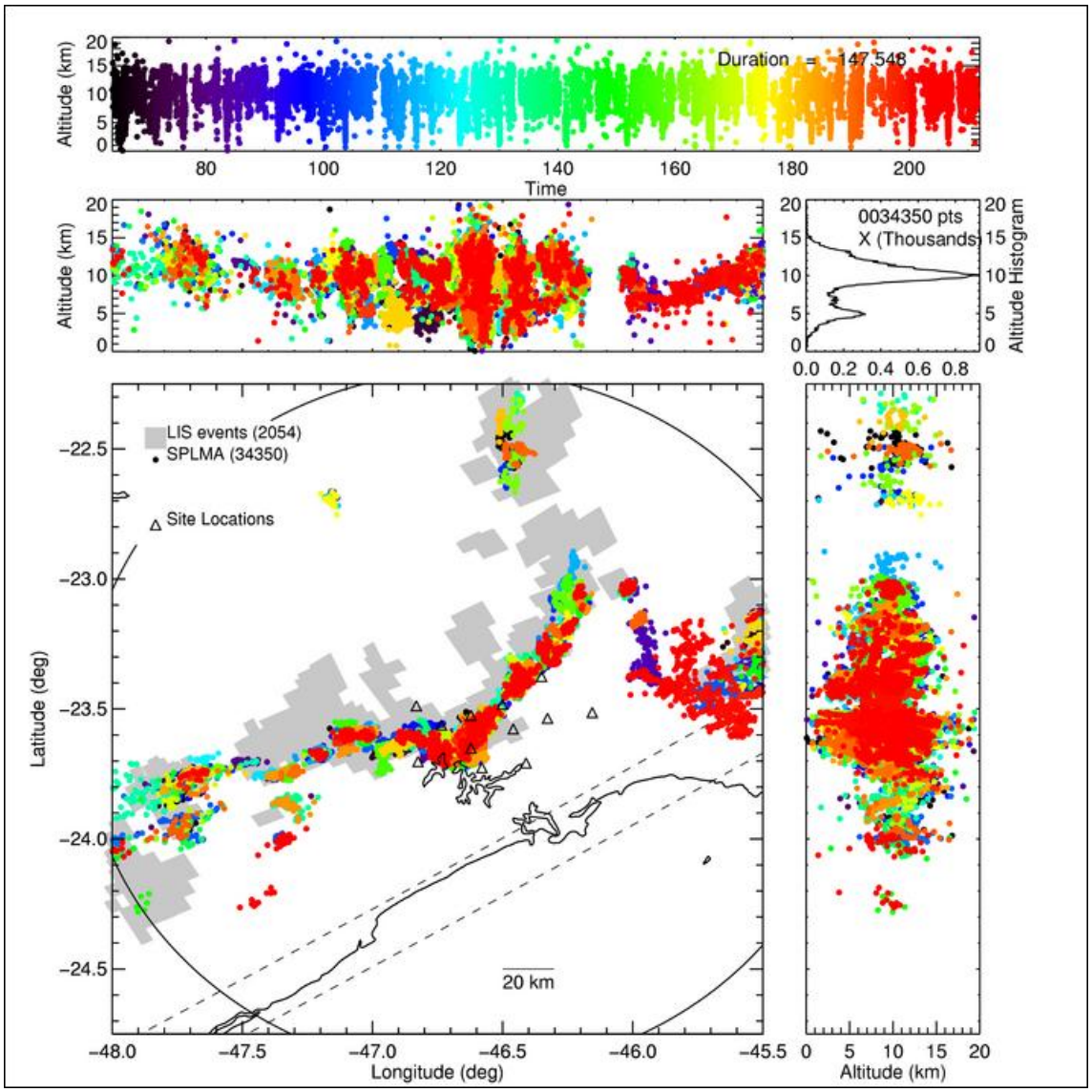

Figure 4: The coincident lightning observations on February 10, 2012 at 1900 UTC during a Lightning Imaging Sensor (LIS) overpass from approximately 19:01:10 to 19:03:24 UTC. The plotted ground-based lightning data are limited both temporally and spatially to the LIS overpass limits. The left panel shows the LIS pixels (grey squares) and the ground strikes detected by LMA VHF sources (the colored dots are function of the time). The projections east–west (top) and north-south (left) as functions of the altitude and the number of sources as a function of the altitude are also shown in the left panel.

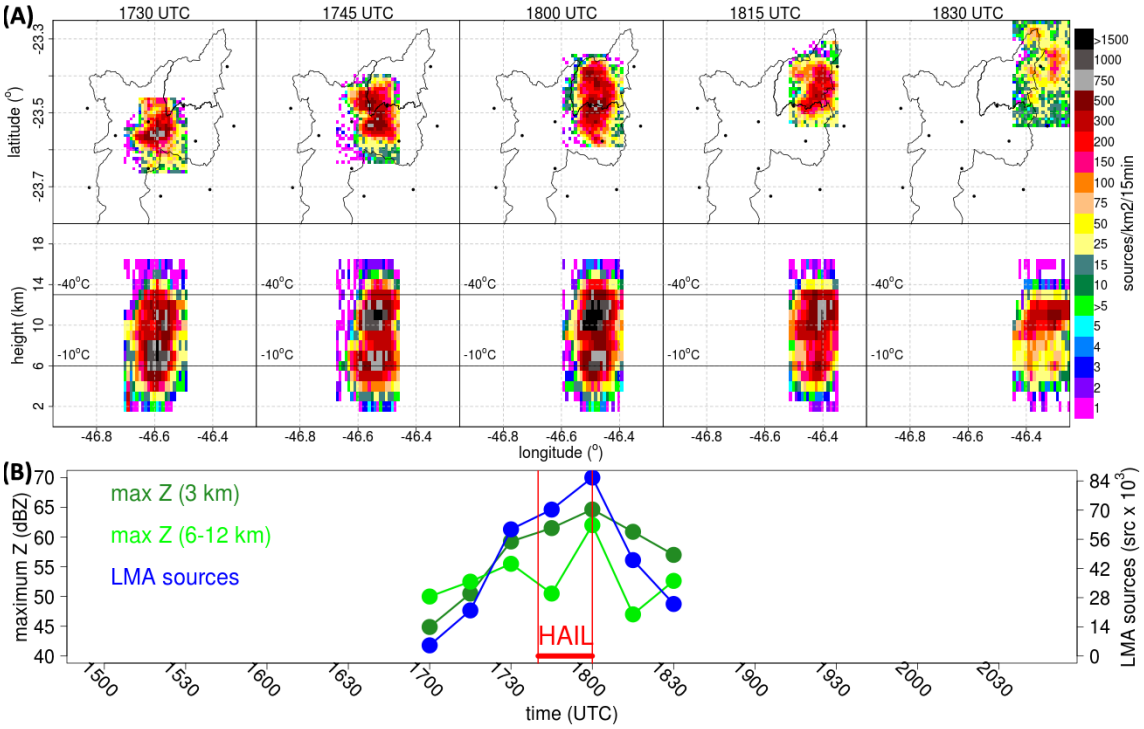

Figure 5: A) Accumulated LMA lightning source density (number of sources in a 1x1 km grid box during a 15-minute period) for a hail-producing convective cell on 7 January 2012. The upper panels show a plan (latitude-longitude) view and the bottom panels show height-longitude views of the convective cell. Horizontal black lines in the bottom panels indicate the approximate heights of the -10°C and -40°C isotherms, where most of the electrical charge transfer occurs. B) Time evolution of the maximum reflectivity and the number of LMA lightning sources. Red lines indicate hail occurrences in São Paulo and Guarulhos (the two cities showed in panels of A). Only data from the hail-producing convective cell are shown.

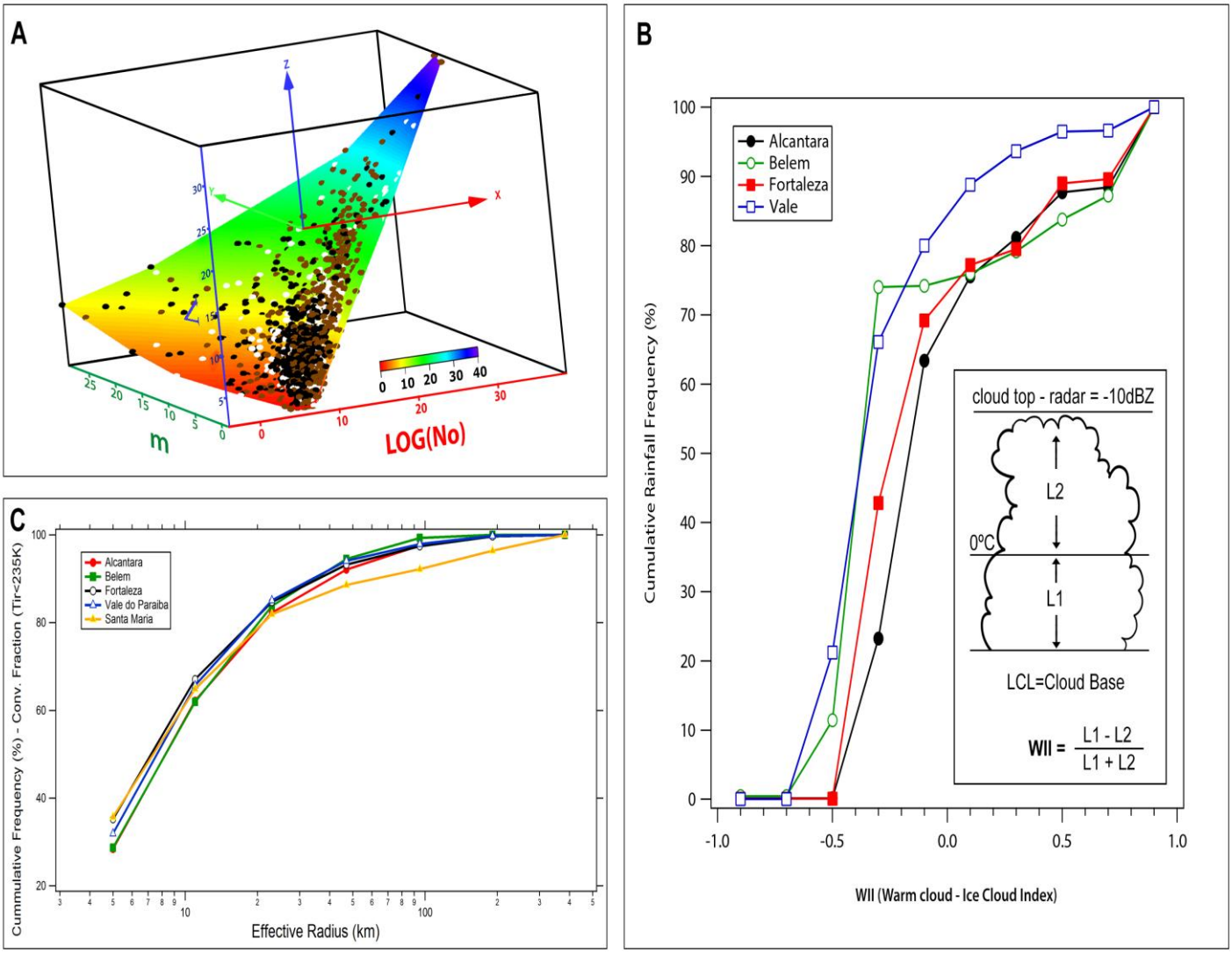

Figure 6: A) The DSD gamma parameters for Vale do Paraiba (black dots), Belem **(brown dots) and Santa Maria (white dots) in the three-dimensional space composed** by N_0, m and Λ. The color of the interpolated surface is associated with the Λ values. B) The cumulative rainfall as a function of the WII (warm cloud–ice cloud index) for Alcantara, Fortaleza, Belem and Vale do Paraiba. LCL stands for lifting condensation level. C) The cumulative convective cloud cover (Tir<235K) as a function of the cloud cluster effective radius for each campaign.

TABLE I: Description of the experiment period, additional instruments and the radars employed during each campaign and a description of the instruments at the main site.

Experiment	Period	Additional Instruments	Radars
Alcantara	2010-03-01 - 2010-03-25	ADIMIRARI Radiometer	EEC X-Band Dual Pol Radar
Fortaleza	2011-04-03 - 2011-04-28		Gematronik Meteor 50DX XPOL Radar
Belem	2011-06-01 - 2011-06-30	Controlled Meteorological balloons and GPS network	Gematronik Meteor 50DX XPOL Radar and S-Band Doppler Radar
Vale do Paraiba	2011-11-01 - 2012-03-31	Lightning detection networks and high-speed cameras.	Gematronik Meteor 50DX XPOL Radar and 2 S-Band Doppler
Santa Maria	2012-11-05 - 2012-12-12	Mesoscale network of automated weather station	IACIT 2 S-Band Doppler Radars
	Main Site		
Instruments	**Manufacture**	**Measurement**	**Retrieval Parameter**
Microwave radiometer	MP3000A (Radiometrics)	35 microwave Brigh. Temp. channels (22-30 and 51-58IR infrared channel (9-11µm)	Temperature, Humidity, Water Vapor Density and Liquid Water profiles and integration
Disdrometer	JOSS-WALDVOGEL (RD-80, Disdromet Ltd.) and PARSIVEL (Ott Inc.)	Drop Size Distribution (DSD) Impact (Joss- Valdwogel) and Laser (Parsivel)	DSD, Rain Rate, Liquid Water Content and Terminal Velocity
Rain Gauge	Tipping buck (Hydrological Services Rain Gage 0.01 inch (0.254mm)	Rainfall	Rain Rate
Vertical Pointing Radar	Micro Rain Radar (MRR-2), vertical pointing - 24.1GHz (METEK)	Doppler spectral	Reflectivity, Rain Rate, Liquid Water Content, Terminal Velocity, and Path-Int. Attenuation
LIDAR	Light Detection and Raging - visible Raman Lidar at 532/604 nm (LB10 D-200, Raymetrics)	Backscattering extinction profile	Cloud and aerosol extinction profile, and cloud thickness
GPS	Trimble NetR8 GNSS receptor dual frequency.	Zenithal Tropospheric delay	Integrated Water Vapor
Surface Tower	Solar Kipp & Zonen instruments, Campbell Scientific and Li-Cor, Inc. weather instruments, CS7500, open path analyzer measuring CO2 and H2O surface fluxes using eddy cov. tech.	Surface weather variables, soil and temperature, radiative budget and CO2 and H2O eddy covariance	Radiative budget, soil temperature and moisture, surface air relative humidity, temperature and wind, moisture, CO2 and heat fluxes.